Influence of loading rate on the mode II fracture toughness of vinyl ester GRP

R. J. Brambleby[a,*], L.A. Louca[a], S.E. Mouring[b]

[a] *Department of Civil and Environmental Engineering, Imperial College London, UK*
[b] *Department of Naval Architecture and Ocean Engineering, United States Naval Academy, Annapolis, USA*

Abstract

Four point bending end notched flexure (4ENF) tests were used to evaluate the mode II fracture toughness (G_{IIC}) of glass fibre reinforced vinyl-ester (GFRP) specimens in order to expose the sensitivity of G_{IIC} to loading rate. Tests were carried out at load displacement rates ranging from 1 to 6000 mm/minute. Finite element models were used to evaluate the correction factors that are required during data reduction in order to compensate for geometrical non-linearity in the test. A high speed video camera was used in conjunction with the digital image correlation technique to measure crack propagation during the tests. It was found that, for short crack lengths, G_{IIC} tended to increase as loading rate was increased.

Keywords: A. Glass fibres, B. Fracture toughness, D. Mechanical testing

1. Introduction

Fibre reinforced polymer composite (FRP) materials can provide excellent performance in terms of strength and stiffness versus weight, as a result they have become important for structural applications in a wide range of industries including automotive, energy and marine. However, due to some critical performance limitations that are exhibited by FRP materials, such as limited ductility, it is often necessary to use FRP in conjunction with metallic components. Typically the metallic component is able to provide the combination of strength and ductility that is required in locations that are subjected to high stresses. In such situations it is necessary to form a load bearing joint between the FRP and metallic components. The present study is part of a project that is investigating the performance of perforated double-lap joints between Glass-fibre Reinforced Polymer (GFRP) and steel. Tests on perforated GFRP-to-steel double-lap joints of the type shown in Figure 1 have demonstrated that the joints exhibit greater tensile strength when tested under impact loading rates than they do under quasi-static loading rates [1]. Finite element (FE) models of the joints indicate that mode II fracture toughness (G_{IIC}) of the

*Principal corresponding author
Email address: reuben.brambleby10@imperial.ac.uk (R. J. Brambleby)

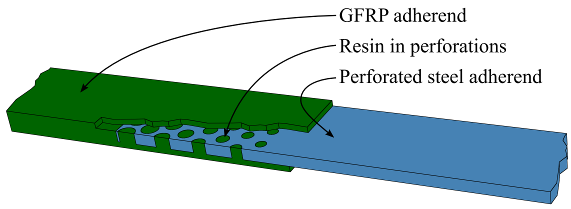

Figure 1: Cut-away view of a co-bonded perforated steel-GFRP double-lap joint [1].

GFRP matrix is the material property that dominates the tensile strength of the perforated joints. We therefore speculate that G_{IIC} of the vinyl-ester polymer resin used in the joint specimens is greater at impact loading rates than at quasi-static loading rates.

There is limited data in the literature regarding the effect that changes in loading rate have on the value of G_{IIC} for vinyl-ester composites. Compston et al [2] investigated loading rate effects on G_{IIC} for unidirectional vinyl-ester GFRP. They generated data for specimens that used five different resins, one un-toughened resin and four toughened resins. They reported that loading rate had no significant effect on G_{IIC}. However, it is worth noting that Compston et al attributed greater significance to their results for maximum toughness ($G_{IIC\text{-max}}$) than they did to their results for crack initiation toughness ($G_{IIC\text{-init}}$). Their results suggest that $G_{IIC\text{-init}}$ increases as loading rate increases for four of the five resins that they tested, including the un-toughened Derakane 411-45 resin. There is significantly more literature regarding the effect of loading rate on G_{IIC} for epoxy-resin composites, although the majority of this covers carbon-fibre rather than glass-fibre composites. The bulk of this literature suggests that G_{IIC} for carbon-fibre epoxy composites (epoxy CFRP) reduces as loading rate increases [3, 4]. An extensive review of the literature was reported by Jacob et al [5] in 2005, they concluded that there appears to be a lack of consensus regarding the influence of loading rate on fracture toughness properties of composite materials.

A more recent study by Guimard et al [6] used physical test results for G_{IIC} over a range of loading rates to show that it is not possible for numerical models to replicate their experimental results unless the cohesive interface used in the numerical model incorporates a rate effect. Guimard et al attribute the apparent increase in G_{IIC} to an increase in microcracks at the crack tip as crack velocity increases.

Verdiere et al [7] studied un-tufted and tufted epoxy CFRP material at various loading rates up to approximately 7 m/s, this is a significantly higher loading rate than the maximum rate used here. They found that there was a significant rate effect on G_{IIC} for the tufted material while there was little rate effect for the un-tufted material.

Marzi et al [8] used reinforced double cantilever beam specimens and reinforced end notched flexure specimens to study the loading rate effect on G_{IC} and G_{IIC} respectively for epoxy CFRP material. They found that for G_{IC} (mode I fracture toughness) there was a strong loading rate effect, while for G_{IIC} no rate effect was detected.

The lack of consensus in the literature regarding the effect of loading rate on G_{IIC} prompted us to carry out the experimental study reported here, in which we perform mode II fracture tests at a range of load displacement rates.

2. Materials and specimen fabrication

The resin, reinforcement and reinforcement orientation used in this study were chosen in order to match those used in the hybrid joints being tested as part of the overall project [1]. The polymer matrix was Dow Derakane 510A-40, an epoxy vinyl ester resin designed to offer a high degree of fire retardance combined with good chemical resistance and toughness [9]. The reinforcement consisted of four plies of Owens Corning TTX1330 fabric, this is a stitch bonded non-crimp tri-axial E-CR glass fabric with areal weights of 520 g/m^2 in the 0° direction and 401 g/m^2 in both the +45° and -45° directions.

A 12.7 micron thick Teflon® film was used to generate an initial debonded region in the specimens as is required for the end-notched flexure test. The reinforcement and debond film were layed up by hand and the vacuum assisted resin transfer moulding (VARTM) process was used to fabricate a single sheet of GFRP material which was then cut into individual specimens using a water-jet cutter. The nominal dimensions of the specimens and the reinforcement layup are shown in Figure 2. The overall length and width of the specimens are as suggested by Hodgkinson [10], the overall thickness is the result of the chosen reinforcement layup, and the length of debond film is in accordance with the DoD Composite Materials Handbook [11]. During fabrication the resin was mixed and cured in accordance with the recommendations of the manufacturer.

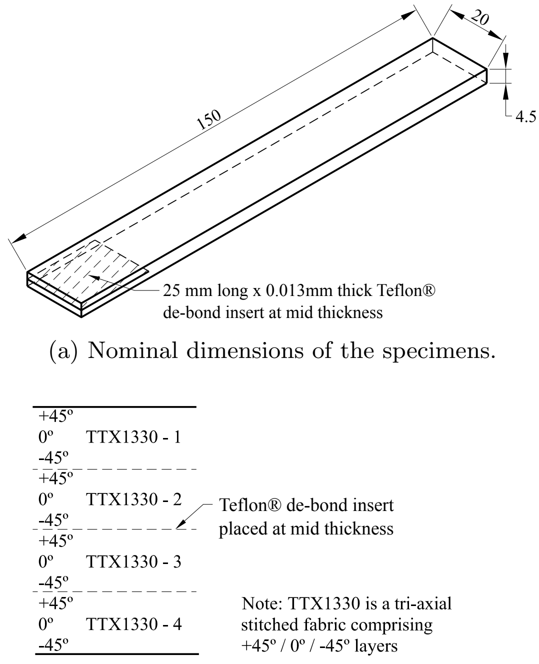

(a) Nominal dimensions of the specimens.

(b) Reinforcement layup of the specimens.

Figure 2: Details of the test specimens.

3. Physical testing

3.1. Test configuration

A variety of test configurations have been proposed for evaluating G_{IIC} of fibre reinforced composite materials [10]. Experimental comparisons of five of the most commonly used configurations are provided by Davies et al [12] and Wang et al [13].

The three point bending end notch flexure (ENF) configuration has the disadvantage of not generating stable crack growth in the specimen [10, 12] while the over notched flexure (ONF) configuration was found to suffer from an increase in frictional effects as crack length grows [13]. The stabilised end notched flexure (SENF) configuration relies on the measurement of crack shear displacement during the test, this measurement is used as feedback to the test machine in such a way as to deliver a constant shear displacement rate during the test [12]. Providing this load control feedback while carrying out a test at a relatively high load displacement rate was considered to be a significant added complexity which made the SENF configurations un-attractive.

The four point bending end notched flexure (4ENF) and end loaded split (ELS) test methods have both been shown to deliver repeatable and reliable results [12, 13] and do not suffer from the disadvantages described above for the ENF, SENF and ONF configurations. However, a standard Instron 4ENF fixture was available to the author and making the necessary modifications to this fixture was considerably more economical than making an ELS fixture. Therefore the 4ENF test configuration was chosen for the tests carried out here.

The 4ENF test was proposed by Martin and Davidson [14] as an improvement on the standard three point bending end-notched flexure (ENF) test. As the name suggests a four point bending fixture is used, see Figures 3 and 4. A 4ENF specimen has a mid-thickness starter crack at one end. The specimen is placed in the test fixture in such a way that the tip of the pre-crack is positioned just inside the inner span of the fixture. During the test, flexural stresses are imposed on the specimen. When these stresses are sufficiently large, then mode II fracture occurs at the crack tip and the mid-thickness crack is forced to propagate further into the specimen. The compliance of the specimen increases due to this crack propagation which leads to a reduction in the flexural stresses and thus crack propagation is arrested. In the context of the current study a significant benefit of using the 4ENF test, as opposed to the ENF test, is that it readily generates stable crack growth during the test. Therefore the rate of crack growth in a 4ENF test tends to be more closely related to the applied rate of load displacement than is the case for the ENF test [10].

A partially custom made four point bending fixture was used for the tests, this is shown in Figure 4. The flexural stiffness of the 4ENF specimen varies along the length of the specimen, this change in flexural stiffness leads to an un-symmetrical deflected shape which must be allowed for by using a pivoting fixture. The pivoting fixture was designed to provide a small vertical offset between the pivot point and the loading points while maintaining visual access to the edge of the specimen. A small vertical offset for the pivot point is required in order to maintain a balanced load at the two loading rollers, visual access to the side of the specimen is required throughout the test in order to monitor crack propagation.

The maximum loading rate used here is slow enough to ensure that the level of kinetic energy in the specimen is small compared with the strain energy. However, inertial effects do influence the measurement of applied load due to the combination of the mass of the hydraulic jaws and the stiffness of the load cell in the test machine. The natural vibration period of the upper jaws and primary load cell was found to be approximately 50 ms while the shortest time between successive steps in the crack propagation was found to be approximately 8 ms. Thus it was not possible to carry out accurate load measurement using the built-in load cell. To overcome this problem the test setup was arranged to place both the low-mass portion of the fixture and a secondary load cell on the static side of the load-string. Using this arrangement the natural vibration period of the load measurement was reduced to approximately 1.5 ms. A low-pass filter was applied to the measured load data in order to attenuate the load oscillations that were caused by vibration in the fixture and load cell. The low pass filter was implemented within a Python [15] script, the effect of applying this filter to the data from a 6000 mm/minute test can be seen in Figure 5.

3.2. Test method

The digital image correlation (DIC) technique was used to measure the length of the propagating crack during the 4ENF tests. It was therefore

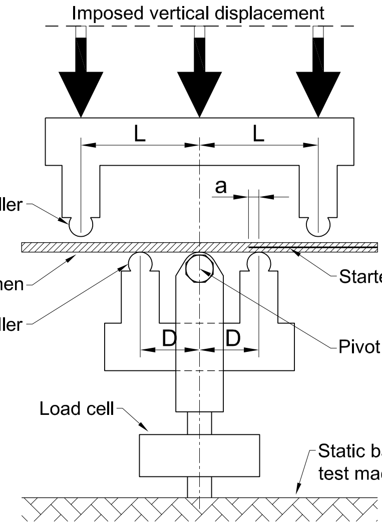

Figure 3: Schematic of the test fixture, D=25mm, L=50mm, a=crack length.

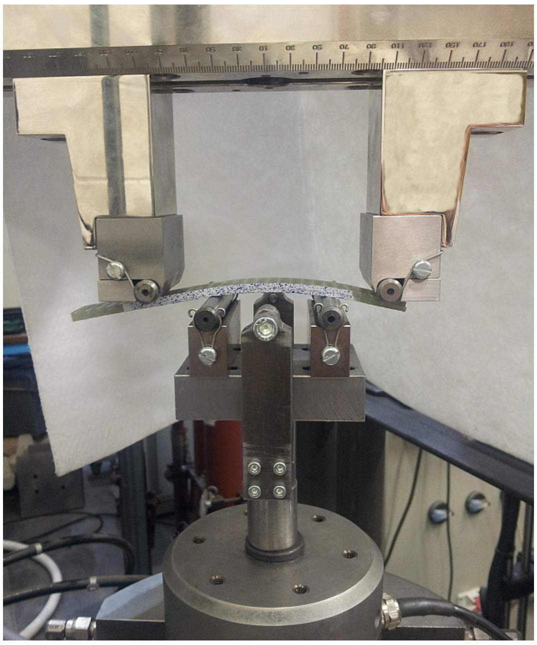

Figure 4: Photo of the fixture in use.

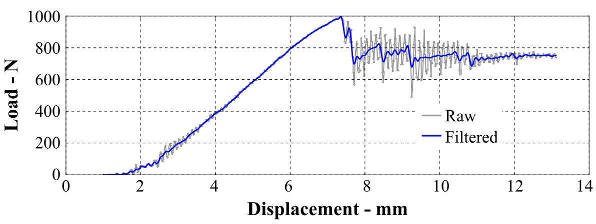

Figure 5: Load versus displacement plot for a specimen tested at 6000 mm/minute showing raw load data and load data after application of a low-pass filter.

necessary to apply a suitable speckle pattern to one edge of each specimen prior to testing. This speckle pattern was achieved by first spraying the edge of each specimen with matte white paint, then using a blow-pen to apply a random speckle onto the white edge.

In each specimen, before the 4ENF test was carried out, a three point bending arrangement and a quasi-static loading rate was used to achieve a controlled length of initial mode II pre-crack beyond the de-bond insert. It has been reported that the resin rich region ahead of the de-bond insert in ENF specimens may cause an artificially high apparent toughness [10]. The initial mode II pre-crack overcomes this problem. As indicated in Figures 6 and 7, the test setup comprises a universal testing machine (UTM), the four point bending fixture, a high speed video camera and a Windows PC with a high speed analogue data acquisition card. The analogue signals from the machine displacement and load transducers are recorded using the data acquisition card. The video frame clock signal from the video camera is used as an external clock for the acquisition card to ensure that the data logging rate is appropriate for the video capture rate. Video clock frequencies ranged from 40 Hz for the slowest tests to 50 kHz for the fastest tests. A trigger switch, which is activated by the moving cross-head of the test machine, is used to trigger the video camera and data acquisition card. An Instron 8802 servo-hydraulic UTM and 25kN Dynacell dynamic

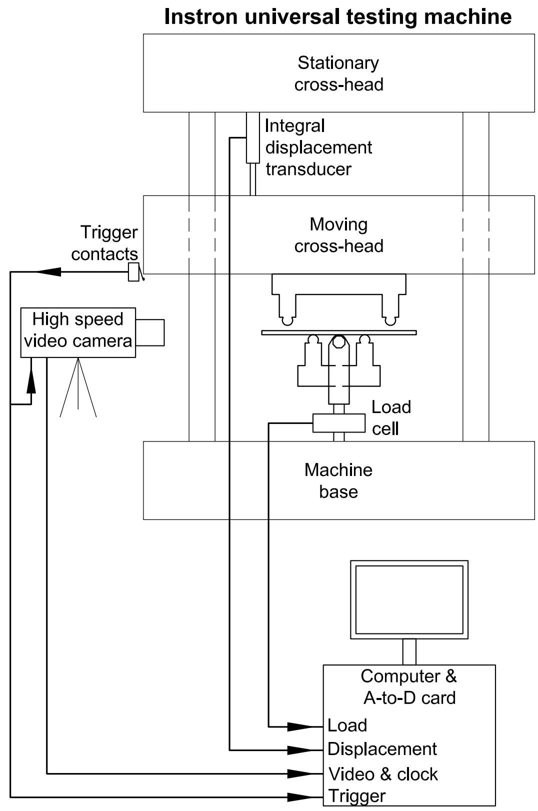

Figure 6: Schematic of the test setup and instrumentation.

load cell were used to carry out tests with nominal displacement rates ranging from 1 mm/minute to 6000 mm/minute. It can be seen in Figure 3 that the setup is arranged to provide a gap between the outer rollers and the specimen before the test starts. This gap allows time for the test machine cross-head to accelerate up to the required displacement rate before load is applied to the specimen. At a load displacement rate of 6000 mm/minute the UTM cross-head takes approximately 25 ms to accelerate up to speed, this relates to approximately 1.5 mm of displacement, typically the first crack propagation event will occur once the cross-head displacement

Figure 7: Photograph showing the fixture, test machine and video camera.

has exceed 5 mm. Once the initial gap is closed and contact is made between the outer rollers and the specimen, then a small re-alignment of the specimen and inner rollers takes place. From the high speed video of a 6000 mm/minute test it can be seen that some chatter vibration of the specimen occurs during this re-alignment and evidence of this vibration can be seen in the plot of raw load data in Figure 5. After the first few millimetres of displacement the chatter vibration is no longer evident and the specimen is in constant contact with all four rollers for the remainder of the test. During the test the inner rollers rotate slightly around the fixture pivot point due to changes in the deflected shape of the specimen as the crack propagates.

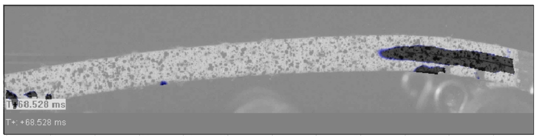

(a) a = 11.6mm

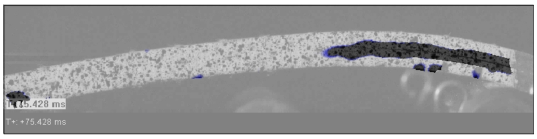

(b) a = 17.5mm

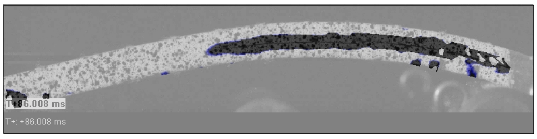

(c) a = 30.6mm

Figure 8: Typical DIC images from a 4ENF test showing crack growth during the test.

3.3. Calibration of DIC crack length measurement

As previously discussed, the DIC technique was used to measure crack propagation during the 4ENF tests. The DIC analysis was carried out using the DaVis software package [16]. Shear strain plots from these DIC analyses were used to identify the mid-thickness crack in the 4ENF specimen, see Figure 8. The DaVis software was used to determine the spatial coordinates of the start, middle and end of the crack, the length of the crack was calculated using these spatial coordinates. The accuracy of this crack measurement technique was checked as follows:

- A previously tested specimen was placed in the fixture.
- A pair of digital vernier calipers were used to accurately determine the position of the specimen relative to the fixture, see Figure 9.
- The video camera was used to capture images of the specimen while a small vertical displace-

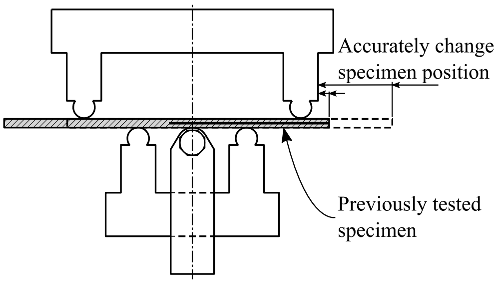

Figure 9: Crack length measurement calibration.

ment was applied.

- This process was repeated for six different measured specimen positions.

The DIC technique was then used to measure the crack tip position for each of the six calibration videos and these crack tip position results were compared with the specimen positions that were measured using the vernier calipers. Thus the accuracy of the DIC measurement technique could be determined. It is worth noting that, as indicated in Equation 1, we are interested in the change in crack length as the test proceeds rather than the absolute crack length. Therefore, during calibration, it is adequate to know the change in crack tip position rather than absolute crack tip position. If we ensure that the displacement applied to the specimen during calibration is too small to increase the length of the crack in the specimen, then the vernier caliper measurements can be used to determine the change in crack tip position. Using this calibration method it was found that the measurement of relative crack length could be achieved with better than ±2% accuracy which was considered to be acceptable.

3.4. Check of fixture compliance

Davidson et al [17] have noted that fixture compliance can be a critical factor for the 4ENF test. The author used the DIC software to measure roller displacement during a 4ENF test and compared these values with the cross-head displacement data that was logged during the test. It was found that cross-head displacement matched roller displacement with an accuracy of approximately ±1.5%. Again this was considered to be acceptable.

3.5. Data reduction

It is common to express the mode II fracture toughness of a composite material in terms of mode II critical energy release rate G_{IIC} [10]. The critical energy release rate can be related to the rate of change of specimen compliance with crack length [18] using equation 1, where P_C is the load required to cause crack propagation, $\frac{dC}{da}$ is the rate of change of specimen compliance with crack length and B is the width of the specimen.

$$G_{IIC} = \frac{P_C^2 \frac{dC}{da}}{2B} \quad (1)$$

The steps required to calculate G_{IIC} from the results collected during a 4ENF test are: 1) measure the specimen width, 2) select critical points in the results data, 3) carry out a DIC analysis of the video captured during the test, 4) determine the crack length for each critical point using the DIC analysis, 5) apply correction to the measured load at each critical point to allow for the effects of

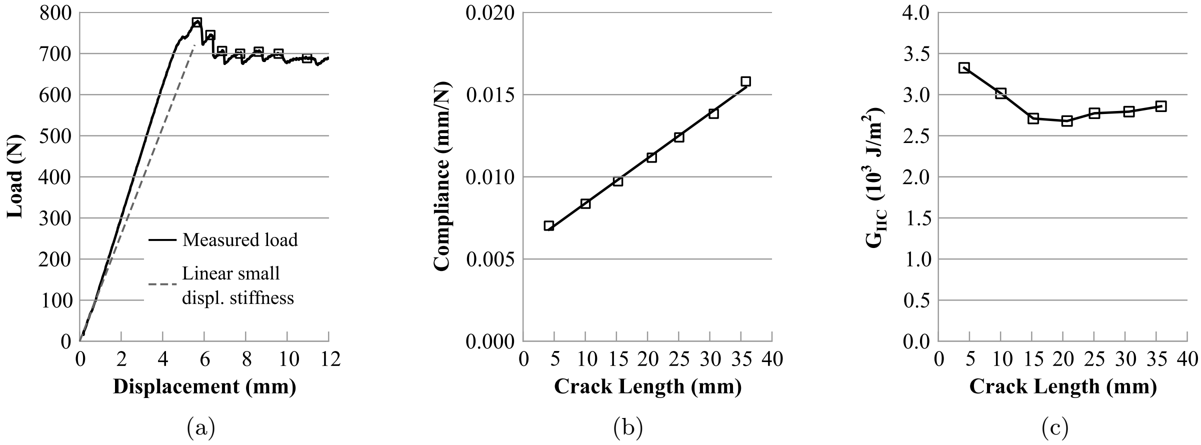

Figure 10: Plots of typical experimental data illustrating the 4ENF data reduction method (50 mm/minute loading rate).

large displacements (see Section 3.6), 6) calculate the specimen compliance at each critical point, 7) apply linear regression to the compliance results to determine the slope of compliance versus crack length and 8) calculate the fracture toughness at each critical point using equation 1. The critical points referred to above are those points in the results data that correspond to peaks in the measured load. These occur just prior to each stepwise crack propagation event. A typical set of plots and numerical data generated during 4ENF data reduction are shown in Figure 10 and Table 1. These help to illustrate the data reduction process and show the drops in applied load that occur at each stepwise crack propagation event.

Crack Length mm	Corrected Load N	Displace- -ment mm	Compli -ance mm/N	Toughness GIIC 10^3 J/m^2
4	698	4.9	0.007	3.33
10	664	5.6	0.008	3.01
15	630	6.1	0.010	2.71
21	626	7.0	0.011	2.68
25	637	7.9	0.012	2.77
31	639	8.8	0.014	2.79
36	647	10.2	0.016	2.86

Table 1: Tabulated experimental data illustrating the 4ENF data reduction method.

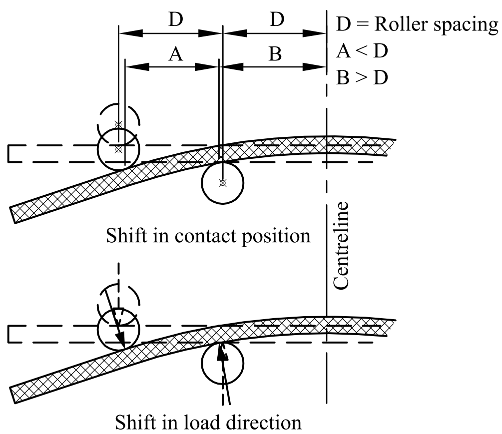

Figure 11: Large displacements during a 4ENF test generate changes in geometry and loading direction.

3.6. Load linearisation

Large displacements occur during the 4ENF test as illustrated in Figure 8. As shown in Figure 11 this large displacement causes geometrical non-linearity in the test setup, the effective roller spacing changes and the direction of loading does not remain vertical. The non-linear load displacement behaviour of the 4ENF test is illustrated in the load versus displacement plot given in Figure 10a, the measured behaviour and the theoretical linear behaviour are both plotted. The change in effective roller spacing causes an apparent increase in stiffness. As the load applied by the rollers rotates away from vertical, the horizontal component of load tends to increase the bending moment in the specimen and, due to the fact that only vertical load is recorded, the apparent stiffness begins to reduce. This effect is illustrated in the fixed crack FE results shown in Figure 12, once deflection exceeds approximately 10 mm the horizontal component of applied load begins to dominate the behaviour causing the apparent stiffness to drop. This geometrical non-linearity must be corrected in order to use the linear elastic fracture toughness equation for G_{IIC}, Equation 1. The load correction factor that must be applied to the experimental data is a function of both displacement and crack length. The load correction factor, shown in Figure 13, is derived from a set of fixed crack length FE models, details of the FE models are given in the following section. Load versus displacement results are generated for six of these fixed crack length models using crack lengths of 0 mm, 7 mm, 14 mm, 21 mm, 28 mm and 35 mm. The method for generating the load correction curve for each fixed crack length model

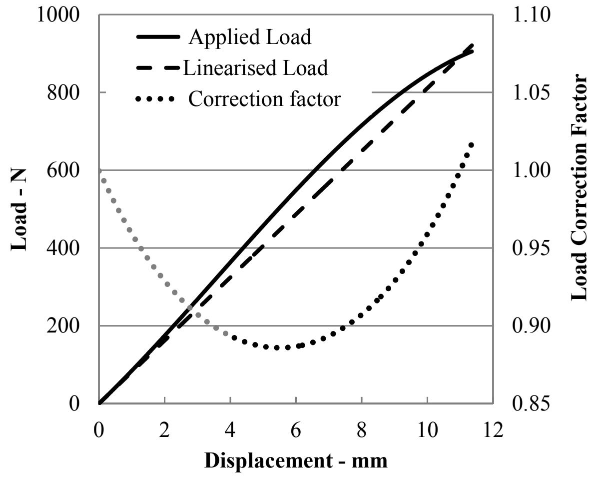

Figure 12: Typical load versus displacement curve for a fixed crack FE model, showing the calculated load correction factor and linearised (corrected) load.

is as follows. Regression analysis is used to fit a quadratic curve to the load versus displacement results from the fixed crack length FE analysis. We know that there should be zero displacement at zero load so this curve is forced to pass through the origin. The regression analysis generates the two polynomial coefficients (A and B) for the curve $P = A\Delta + B\Delta^2$, where P is the applied load and Δ is the corresponding displacement. The coefficient A gives the initial slope of the curve, this is the small displacement flexural stiffness so we take this to be the flexural stiffness of a specimen with the given crack length. We can now define the load correction curve as $C_L = \frac{A\Delta}{P}$, where C_L is the correction factor for crack length L and the remaining terms are as previously defined.

The load correction curve for a crack length of 21 mm is shown on Figure 12. The curve is given for the full range of Δ, but we do not use the por-

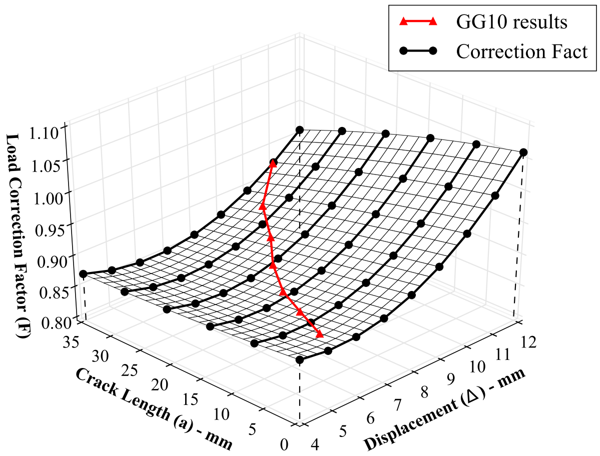

Figure 13: Plot of the load correction factor surface ($F(a, \Delta)$). Results for a typical specimen are plotted on the surface.

tion for $\Delta < 4$ mm due to the fact that cracks in the physical tests do not begin to propagate until the displacement exceeds approximately 5 mm. Load correction curves are determined for each of the six fixed crack length models and the resulting correction curves are used to generate the continuous correction surface shown in Figure 13. Regression analysis is used to fit a set of third order polynomials in order to develop the surface along the crack-length axis. The crack propagation data points for a physical 4ENF test are also shown on Figure 13 in order to indicate the path of a typical set of results across the correction surface.

The load correction surface is used to determine the load correction factor that is required for each critical point of a 4ENF test. The displacement and crack length corresponding to the given critical point define the required location on the correction factor surface and thus the required load correction factor. Once the corrected loads are calculated for each data point then these can be used with Equation 1 in the standard manner [10]. This load linearisation method has been tested on crack propagation FE models for crack propagation lengths from 0 mm to 35 mm. The calculated value of G_{IIC} over this range is within approximately $\pm 2\%$ of the value used in the corresponding Abaqus cohesive traction-separation material definition.

4. Numerical modelling of the 4ENF test

4.1. Crack propagation FE models

A 2D plane strain FE analysis of the 4ENF test was carried out using the dynamic explicit procedure within Abaqus 6.12 [19]. The overall specimen thickness of 4.1 mm comprises 2 mm thick upper and lower GFRP regions and a 0.1 mm thick cohesive region as illustrated in Figure 14. The thickness of both the cohesive and pre-crack regions in Figure 14 have been artificially exaggerated to aid clarity. The pre-cracked region of the specimen was modelled using a 0.1 mm thick layer of GFRP material which had frictionless surface-to-surface contact with the upper and lower GFRP regions. The 0.1 mm thick pre-crack layer was kept in position by applying a rigid tie between the node at one corner and the adjacent node in the lower GFRP region.

The GFRP material was modelled using 4 node plane stress CPS4R elements while the cohesive material was modelled using 4 node cohesive COH2D4 elements. The stiffness and progressive failure of

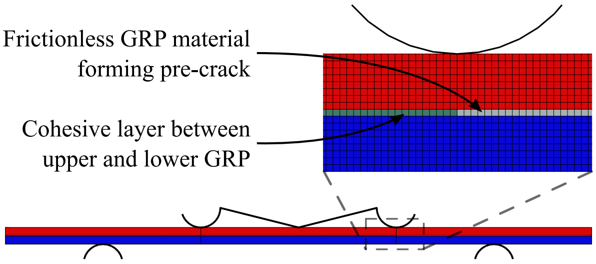

Figure 14: FE model of the 4ENF test.

Flexural modulus N/mm^2	Poisson's ratio	Density kg/m^3
20,000	0.36	2200

Table 2: Properties for the GFRP material used in the FE models.

the cohesive layer was modelled using the Abaqus traction-separation behaviour with linear stiffness degradation [19]. The support rollers were modelled as analytical rigid parts using circular arcs of 10 mm diameter to match the rollers used in the test fixture. The pivoting portion of the 4ENF fixture, which incorporates the load rollers, was modelled as a single analytical rigid part with a central pivot point and 10 mm diameter rollers. The material properties and cohesive parameters used for the FE model are given in Tables 2 and 3.

A mesh sensitivity analysis was undertaken using both 4 node linear elements and 6 node quadratic elements. It was found that the governing factor for determining the maximum acceptable mesh size was related to contact discretisation noise rather than bending stiffness or bending stress, if the element size is too large then the load displacement response tends to become stepped. This is due to the interaction of the discretised surfaces. The contact stresses between the rollers and GFRP do not transfer smoothly from one node to the next but display a stick-slip type of behaviour as contact is transferred from one node to the next. It is the avoidance of these stepped load and displacement responses that drove the element size down, a smaller mesh size leads to smaller steps in the response. Having established that a mesh size of 0.25 mm x 0.25 mm provided an acceptably low level of discretisation noise, then a mesh sensitivity analysis was carried out. This analysis has shown that a square mesh with 0.25 mm side length using linear elements provides good accuracy in terms of the stiffness of the model.

The FE model was used to assess the influence that specimen inertia has on G_{IIC} measurements carried out using the 4ENF test setup. At a loading rate of 6000 mm/minute the total kinetic energy in the FE model varies from 0.5x10^{-3} J to 0.8x10^{-3} J with an average value of 0.7x10^{-3} J. If we consider the experimental data given in Table 1, the G_{IIC} crack surface energy related to a 4 mm crack length in the 20 mm wide specimen is approximately 0.3 J and the G_{IIC} surface energy related to a 36 mm crack length is approximately 1.9 J. Thus we can see that the kinetic energy in the specimen is negligible with a value that is approximately 0.2% of the G_{IIC} crack surface energy for the first critical point in a typical 4ENF test.

Figure 15 shows results from both the FE model

	Mode I	Mode II
Energy (10^3 J/m^2)	0.75	2.8
Stiffness (N/mm)	10,000	4,000
Initiation (N/mm^2)	10	30

Table 3: Parameters for the cohesive element traction-separation law used in the FE model.

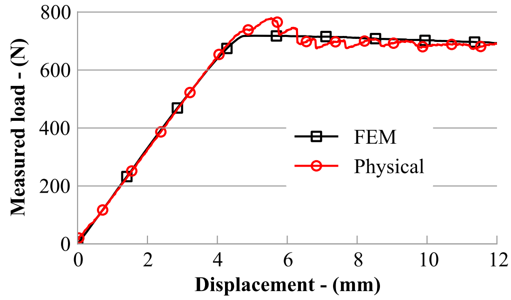

(a) Load versus displacement plot comparing physical and FE model results.

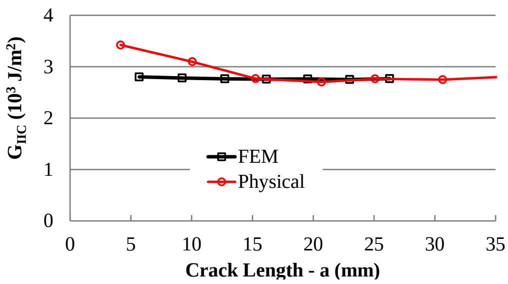

(b) Toughness versus crack length plot comparing physical and FE model results.

Figure 15: Comparison of the behaviour of the FE model and a test specimen.

and one of the physical specimens which was tested at a load displacement rate of 50 mm/minute. It can be seen that there is generally good agreement between the FE and physical results although the FE model does not predict the high initial toughness of the physical test nor the stepwise crack propagation.

4.2. *Fixed crack length FE models*

As previously described, a set of fixed crack length FE models were used to generate the load correction data that is required in order to correct for the large displacement non-linearity of the 4ENF setup. The geometry of each of the fixed crack length FE models is the same as the crack propagation model except that the length of the cohesive layer is adjusted in order to mimic crack lengths ranging from 0 mm up to 35 mm.

Figure 16 shows the 7 mm fixed crack model. It can be seen that the cohesive layer in this model has been shortened in order to create the 7 mm gap between the cohesive material and the pre-crack filler material. The intensity of flexural stress is also shown in Figure 16. The changes in flexural

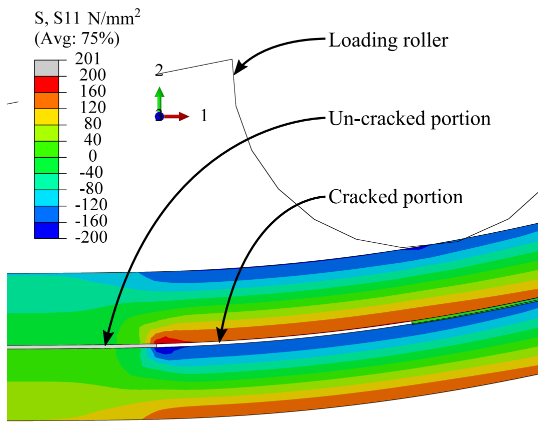

Figure 16: Extract of fixed crack FE model showing the change in flexural stresses at the crack tip.

stress clearly show the transition from the pre-crack region, where the upper and lower arms act independently, to the un-cracked region, where the cohesive layer causes the upper and lower arms to act monolithically. In order to prevent crack propagation in the fixed crack models, the cohesive material is given an artificially high initiation stress. As a result no cohesive stiffness degradation occurs and a fixed crack length is achieved.

4.3. Effects of friction

It has been shown [20] that friction within a 4ENF specimen can have a significant effect on the perceived G_{IIC} for some specimen geometries. The effects of friction on the 4ENF specimens tested here have been investigated by modifying both the fixed crack length and the crack propagation FE models. In each case the Abaqus contact property definition that defines the interaction between the pre-crack filler material and the upper and lower arms of the specimen have been modified to incorporate a classical Coulomb friction model [21] using the penalty friction formulation [19] as outlined in Table 4. It is only necessary to incorporate the friction model within the pre-crack region because the surfaces of the cracked region do not come into contact with one another over the load point displacement range that we have considered here. The classical friction model is defined using a constant coefficient of friction $\mu = 0.35$. This value for μ was established by Davidson et al [17] for carbon/epoxy material with teflon inserts using a hinged plate sliding block test set-up.

	Normal Behaviour	Tangential Behaviour
Friction free	Hard contact	Frictionless formulation
Frictional	Hard contact	Penalty formulation

Table 4: Abaqus contact property options used to define friction free and frictional surfaces in the FE models.

As expected the fixed crack models that incorporated friction were found to be marginally stiffer than the friction free models. However, when the frictional models were used to generate a set of load correction curves, these curves were negligibly different from the correction curves generated using the friction free models. Therefore friction has a negligible effect on the load linearisation curves.

Table 5 shows the relative magnitude of the external work done, cohesive surface damage energy and frictional dissipation energy for a crack propagation FE model in which the load point displacement and crack length have reached values of 11 mm and 35 mm respectively. Approximately 11% of the external work has been dissipated as surface friction and this is reflected in the corresponding apparent fracture toughness value of $G_{IIC} = 3.0kJ/m^2$ compared with the cohesive traction-separation energy of $G_{IIC} = 2.8kJ/m^2$ that was defined in the model. This increase in apparent toughness is similar to that reported by others [22, 23], the importance of this over estimation on our findings is discussed in Section 6.

External Work Nmm	Crack Propagation Energy (Damage) Nmm	Frictional Dissipation Energy, $\mu = 0.35$ Nmm
6216	1992	216

Table 5: External work, damage energy and frictional energy for a crack propagation FE model incorporating interface friction.

5. Results

The load versus displacement and toughness versus displacement results of three typical test specimens are shown in Figure 17. The specimens were tested at nominal loading rates of 50 mm/minute, 750 mm/minute and 6000 mm/minute respectively. The markers in Figure 17a are simply to aid in the identification of the data, while the markers in Figure 17b identify the critical data points for each specimen. Thus, each marker in Figure 17b represents the start of a crack propagation event. The plots in Figure 17 exhibit behaviour that is typical of all specimens, showing a linear response up to an applied load of approximately 500N and a higher initial toughness which falls away as crack length increases.

The initial and average toughness values for each specimen are given in Table 6 and plotted in Figure 18. The initial value is the toughness calculated for the first critical data point, the average value is the toughness averaged over all the critical data points for a given specimen.

While there is significant scatter in the data, a linear regression analysis of the data suggests a 15% increase in the initial mode II toughness over the

Specimen	Loading rate mm/min	Toughness 10^3 J/m^2 Initial	Toughness 10^3 J/m^2 Average
1	1	2.90	2.51
2	1	2.96	2.57
3	1	3.54	3.25
4	50	3.64	3.31
5	50	3.42	2.90
6	50	3.76	3.17
7	50	3.61	2.88
8	349	3.11	2.82
9	350	3.31	3.01
10	352	3.65	3.15
11	749	3.60	2.96
12	749	4.22	3.80
13	747	3.27	3.13
14	3020	3.10	2.45
15	6033	4.35	3.49
16	6052	3.99	2.72
17	6040	3.44	2.67
18	6055	3.79	3.09

Table 6: Fracture toughness versus loading rate results.

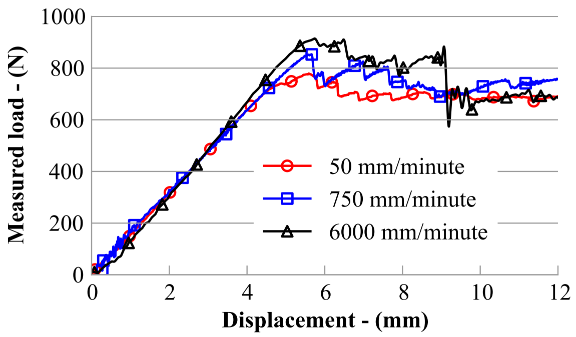

(a) Measured load versus displacement.

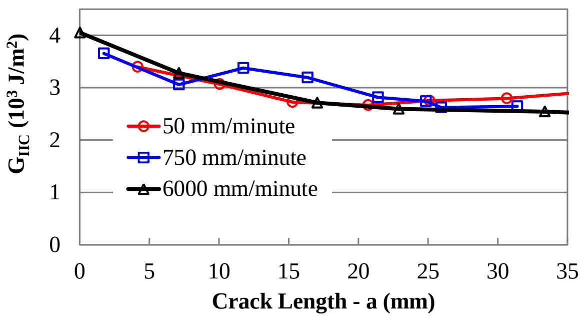

(b) Mode II toughness versus crack length.

Figure 17: Results for specimens tested at 50 mm/minute, 750 mm/minute & 6000 mm/minute.

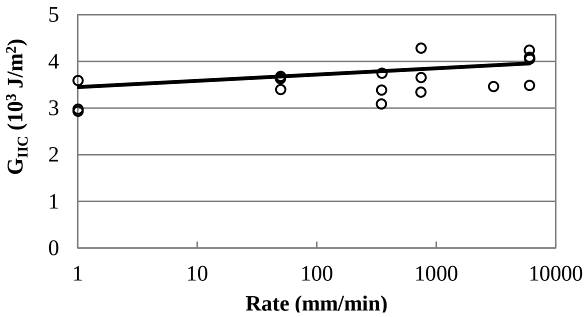

(a) Initial toughness versus loading rate.

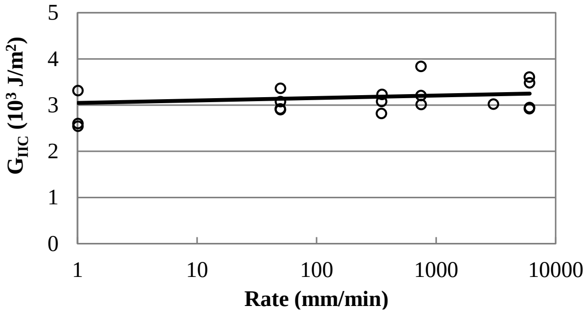

(b) Average toughness versus loading rate.

Figure 18: Fracture toughness versus loading rate results.

loading rate range of 1 mm/min to 6000 mm/min. In comparison, the values for average mode II toughness appear to be much less dependent on loading rate, a linear regression analysis suggests a 7% increase in average mode II toughness.

6. Discussion and conclusions

The 4ENF test method was used to carry out measurements of G_{IIC} of a vinyl ester GFRP material at load displacement rates ranging from 1 mm/minute to 6000 mm/minute. Finite element models of the 4ENF test were used to a) find the correction coefficients that are required to compensate for large deflection non-linearity in the physical tests, b) to assess the importance of inertial effects at the higher loading rates and c) to assess the influence of crack face friction on measured mode II toughness. By applying the calculated large deflection correction coefficients to FE analysis data, it was found that approximately 2% linearisation accuracy could be achieved. By comparing inertial energy with cohesive damage energy of the FE model that had a load displacement rate of 6000 mm/min, it was found that the inertial effects are negligible.

It was found that crack face friction is likely to have an important effect on the apparent mode II toughness of the specimens tested here. However, according to the classical laws of friction [21] the static coefficient of friction, μ_s, is greater than the kinetic coefficient of friction, μ_k, and also μ_k is independent of sliding velocity. If we consider these two laws in conjunction with the fact that crack face friction increases the apparent mode II toughness, we can see that crack face friction is not causing the rate effect on mode II toughness that has been observed here.

The results suggest that there is a loading rate effect on the initial G_{IIC} of Derakane 510A-40 vinyl ester GFRP. It is likely that this loading rate effect on G_{IIC} is a significant contributing factor to the higher tensile strength of perforated double-lap joints tested at higher rates of loading which has been observed in previous testing [1].

The cause of the apparent drop in mode II toughness as crack length increases is not known, but it is apparent from the videos of the physical tests that the crack tends to open under large displacements and also that the crack tended to migrate away from the mid-thickness of the specimen and towards the tension face. The tendency for the crack to open may be caused by a combination of debris within the crack and interference between the rough crack surfaces above and below the crack itself. The opening of the crack will tend to induce mode I fracture in addition to the intended mode II fracture. This mixed mode fracture will modify the measured apparent toughness. The crack opening is only visually apparent at larger displacements, but the tendency to induce some mode I fracture may also be occurring at smaller displacements, thus influencing the apparent toughness.

The use of the high speed video camera and subsequent DIC analysis of the specimens appeared to provide a reliable, effective and convenient method for measuring the crack propagation at all displacement rates.

In terms of future specimen design, it would have been beneficial to use smooth platens for both faces of the specimens during the VARTM process in order to provide a smooth surface on both the top and bottom of the specimens. This would reduce the effects of friction between the specimen and the fixture rollers.

7. Funding

Funding for the work described here was gratefully received from the Office of Naval Research, Arlington, USA (Grant Nos. N00014-12-1-0563 and N00014-15-WX-0-1446).

8. Acknowldgements

The authors would like to thank the team at TSD, Project Support Branch, US Naval Academy under the guidance of Mr Doug Loup, Naval Surface Warfare Center Carderock Division for fabricating the specimens used in the experiments and Andy Pullen at Imperial College London for his assistance in the experimental work.

9. References

[1] R. J. Brambleby, L. A. Louca, and S. E. Mouring. Dynamic strength testing of perforated steel - grp double lap joints. In *ECCM-16 European Conference on Composite Materials*. ESCM, 2014.

[2] P. Compston, P. Y. B. Jar, P. J. Burchill, and K. Takahashi. The effect of matrix toughness and loading rate on the mode-ii interlaminar fracture toughness of glass-fibre/vinyl-ester composites. *Composites Science and Technology*, 61(2):321–333, 2001.

[3] A. J. Smiley and R. B. Pipes. Rate sensitivity of mode ii interlaminar fracture toughness in graphite/epoxy and graphite/peek composite materials. *Composites Science and Technology*, 29(1):1–15, 1987. Cited By :36 Export Date: 22 January 2015.

[4] T. Kusaka, Y. Yamauchi, and T. Kurokawa. Effects of strain rate on mode ii interlaminar fracture toughness in carbon-fibre/epoxy laminated composites. *Le Journal de Physique IV*, 4(8):C8–671–C8–676, 1994.

[5] George C. Jacob, J. Michael Starbuck, John F. Fellers, Srdan Simunovic, and Raymond G. Boeman. The effect of loading rate on the fracture toughness of fiber reinforced polymer composites. *Journal of Applied Polymer Science*, 96(3):899–904, 2005.

[6] Jean-Mathieu Guimard, Olivier Allix, Nicolas Pechnik, and Pascal Thvenet. Characterization and modeling of rate effects in the dynamic propagation of mode-ii delamination in composite laminates. *International journal of fracture*, 160(1):55–71, 2009.

[7] M. Colin de Verdiere, A. A. Skordos, A. C. Walton, and Michael May. Influence of loading rate on the delamination response of untufted and tufted carbon epoxy non-crimp fabric composites/mode ii. *Engineering fracture mechanics*, 96:1–10, 2012.

[8] S. Marzi. Fracture mechanical investigations and cohesive zone failure modelling on automotive composites. *Composite structures*, 111:324–31, 2014.

[9] Ashland Inc. Derakane 510a-40 epoxy vinyl ester resin technical datasheet, 9 August 2008.

[10] J.M. Hodgkinson. *Mechanical Testing of Advanced Composites*. Woodhead Publishing, Cambridge, 2010.

[11] Department of Defense. *Composite Materials Handbook*, volume 1. Polymer matrix composites guidelines for characterization of structural materials. 2002.

[12] P. Davies. Comparison of test configurations for determination of mode ii interlaminar fracture toughness results from international collaborative test programme. *Plastics, rubber, and composites : PRC.*, 28(9):432–7, 1999.

[13] Wen-Xue Wang, Miko Nakata, Yoshihiro Takao, and Terutake Matsubara. Experimental investigation on test methods for mode ii interlaminar fracture testing of carbon fiber reinforced composites. *Composites Part A: Applied Science and Manufacturing*, 40(9):1447–1455, 2009.

[14] R.H. Martin and B.D. Davidson. Mode ii fracture toughness evaluation using four point bend, end notched flexure test. *Plastics, rubber, and composites : PRC.*, 28(8):401–6, 1999.

[15] Python Software Foundation. Python programming language, 2012.

[16] LaVision GmbH. Davis imaging software, version 8.2.2.

[17] B. D. Davidson, X. Sun, and A. J. Vinciquerra. Influences of friction, geometric nonlinearities, and fixture compliance on experimentally observed toughnesses from three and four-point bend end-notched flexure tests. *Journal of Composite Materials*, 41(10):1177–1196, 2007.

[18] D. Broek. *Elementary Engineering Fracture Mechanics*. Kluwer Academic Publishers, Dordrecht, 2002.

[19] Dassault Systemes Simulia Corp. Abaqus 6.12 analysis user's manual, 2012.

[20] Xuekun Sun and Barry D. Davidson. Numerical evaluation of the effects of friction and geometric nonlinearities on the energy release rate in three- and four-point bend end-notched flexure tests. *Engineering Fracture Mechanics*, 73(10):1343–1361, 2006.

[21] J. T. Oden and J. A. C. Martins. Models and computational methods for dynamic friction phenomena. *Computer Methods in Applied Mechanics and Engineering*, 52(1):527–634, 1985.

[22] C. Schuecker and B. D. Davidson. Effect of friction on the perceived mode ii delamination toughness from three- and four-point bend end-notched flexure tests. *ASTM Special Technical Publication*, (1383):334–344, 2000. Cited By :15 Export Date: 7 April 2015.

[23] Hiroshi Yoshihara. Theoretical analysis of 4-enf tests for mode ii fracturing in wood by finite element method. *Engineering fracture mechanics*, 75(2):290–296, 2008.